

# A Method to Estimate Biomechanics and Mechanical Properties of Optic Nerve Head Tissues From Parameters Measurable Using Optical Coherence Tomography

I. A. Sigal\*, J. L. Grimm, J. S. Schuman, L. Kagemann, H. Ishikawa, and G. Wollstein

**Abstract**—Optic nerve head (ONH) tissue properties and biomechanics remain mostly unmeasurable in the experiment. We hypothesized that these can be estimated numerically from ocular parameters measurable *in vivo* with optical coherence tomography (OCT). Using parametric models representing human ONHs we simulated acute intraocular pressure (IOP) increases (10 mmHg). Statistical models were fit to predict, from OCT-measurable parameters, 15 outputs, including ONH tissue properties, stresses, and deformations. The calculations were repeated adding parameters that have recently been proposed as potentially measurable with OCT. We evaluated the sensitivity of the predictions to variations in the experimental parameters. Excellent fits were obtained to predict all outputs from the experimental parameters, with cross-validated  $R^2$ s between 0.957 and 0.998. Incorporating the potentially measurable parameters improved fits significantly. Predictions of tissue stiffness were accurate to within 0.66 MPa for the sclera and 0.24 MPa for the lamina cribrosa. Predictions of strains and stresses were accurate to within 0.62% and 4.9 kPa, respectively. Estimates of ONH biomechanics and tissue properties can be obtained quickly from OCT measurements using an applet that we make freely available. These estimates may improve understanding of the eye sensitivity to IOP and assessment of patient risk for development or progression of glaucoma.

**Index Terms**—Biomechanics, finite element models, glaucoma, intraocular pressure (IOP), inverse modeling, lamina cribrosa (LC), optic nerve head (ONH), strain, stress.

Manuscript received October 16, 2013; revised February 03, 2014; accepted February 10, 2014. Date of publication March 14, 2014; date of current version May 29, 2014. This work was supported in part by National Institutes of Health under Grant P30-EY008098, in part by the Eye and Ear Foundation, and in part by unrestricted grants from Research to Prevent Blindness. G. Wollstein is a consultant to Allergan. J. S. Schuman received royalties for intellectual property licensed by Massachusetts Institute of Technology to Zeiss. *Asterisk indicates corresponding author.*

This paper has supplementary downloadable material available at <http://ieeexplore.ieee.org>, provided by the authors.

\*I. A. Sigal is with the Departments of Ophthalmology and Bioengineering, University of Pittsburgh, Pittsburgh, PA 15213 USA and also with the McGowan Institute for Regenerative Science, Pittsburgh, PA 15219 USA (e-mail: sigalia@upmc.edu).

J. L. Grimm is with the Department of Ophthalmology, University of Pittsburgh, Pittsburgh, PA 15213 USA.

J. S. Schumann is with the Departments of Ophthalmology and Bioengineering, University of Pittsburgh, Pittsburgh, PA 15213 USA, and also with the McGowan Institute for Regenerative Science, Pittsburgh, PA 15219 USA, and also with the Fox Center for Vision Restoration, University of Pittsburgh Medical Center and the University of Pittsburgh, Pittsburgh, PA 15213 USA.

L. Kagemann and H. Ishikawa are with the Departments of Ophthalmology and Bioengineering, University of Pittsburgh, Pittsburgh, PA 15213 USA.

G. Wollstein is Department of Ophthalmology, University of Pittsburgh, Pittsburgh, PA 15213 USA, and also with the Fox Center for Vision Restoration, University of Pittsburgh Medical Center, and the University of Pittsburgh, Pittsburgh, PA 15213 USA.

Digital Object Identifier 10.1109/TMI.2014.2312133

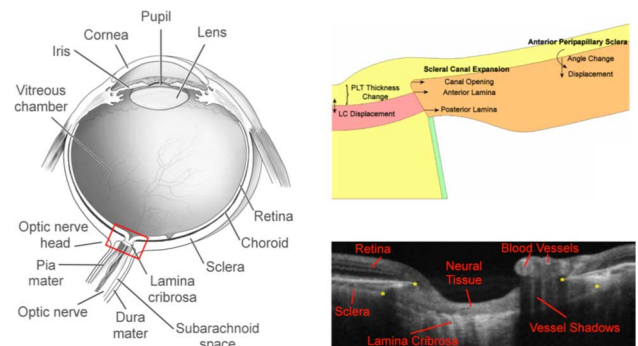


Fig. 1. Human eye, optical coherence tomography, and the model of the ONH. (Left) Schematic cross-section through a human eye. Retinal ganglion cell axons transmit visual information to the brain. These fibers converge at the optic nerve head region (red rectangle), exit the eye through the scleral canal, passing through the LC, and form the optic nerve. The vitreous chamber is filled with the vitreous humor, which exerts the intraocular pressure (IOP) on the interior surface of the tissues. Adapted from a diagram by the National Eye Institute. (Bottom right) Example image of the optic nerve head region acquired with a swept-source OCT. Yellow dots denote landmarks of the canal opening and anterior LC insertion into the sclera. (Top right) Example of the generic axisymmetric model of the ONH used for analysis. Five tissue regions were modeled in detail: sclera (orange), prelaminar tissue (PLT, yellow), lamina cribrosa (LC, red), postlaminar tissue (yellow), and pia mater (green). Also shown are the IOP-induced deformation parameters analyzed for each model. Anterior sclera displacement and rotations (angle change) were extracted at 1.7 mm and 3.0 mm of the axis of symmetry. For clarity only the measurements at 3.0 mm are shown.

## I. INTRODUCTION

LOSS of vision in glaucoma, one of the leading causes of blindness worldwide, is due to death of the retinal ganglion cells and their axons that transmit visual information from the retina to the brain [4]. This damage is believed to initiate at the lamina cribrosa (LC), a structure within the optic nerve head (ONH) in the posterior pole of the eye (Fig. 1) [5], [6]. Elevated intraocular pressure (IOP) is the primary risk factor for the development and progression of glaucoma, and IOP reduction remains the only proven way to preserve vision [5]. This observation, in conjunction with many others [4], [5], [7] strongly suggest that the biomechanical effects of IOP on the tissues of the ONH are central to the disease [5], [6], and have therefore been the focus of numerous recent studies [3], [7]–[10]. Due to the difficulties in accessing the ONH directly for *in vivo* experimentation, much of what is known about ONH biomechanics has been learned through *ex vivo* experiments [3], [9], [11]–[15]

TABLE I

CHARACTERISTICS OF THE EYE GROUPED INTO THOSE FROM THE EXPERIMENT AND THOSE TO BE PREDICTED. THE FIRST OBJECTIVE OF THIS WORK WAS TO USE THE PARAMETERS ON THE LEFT HAND AND MIDDLE COLUMNS TO ESTIMATE THOSE ON THE RIGHT HAND COLUMN. WE CONSIDERED A PARAMETER MEASURABLE WHEN IT HAS BEEN REPORTED CONSISTENTLY AS SUCH IN THE PEER-REVIEWED LITERATURE, AND POTENTIALLY MEASURABLE IF IT HAS ONLY RECENTLY BEEN PROPOSED OR IF IT HAS BEEN USED INFREQUENTLY. THE OUTPUTS OF INTEREST WERE SELECTED BECAUSE THEY HAVE BEEN PROPOSED TO BE IMPORTANT ASPECTS OF ONH BIOMECHANICS, BUT CANNOT YET BE MEASURED IN AN EXPERIMENT *IN VIVO*. PARAMETERS ARE COLORED ACCORDING TO WHETHER THEY ARE INPUTS (GREEN) OR OUTPUTS (BLUE) TO DIRECT FE MODELING (TABLE II). AS IMAGING AND ANALYSIS ADVANCE WE ANTICIPATE THE COLUMNS TO CHANGE, WITH PARAMETERS MOVING TO THE LEFT

Parameters from the experiment		Parameters predicted
Measurable	Potentially Measurable	
IOP	Anterior LC Radius[21]	<b>ONH Biomechanics</b>
Eye Radius	SC Expansion at Anterior LC[28]	Stresses
Scleral Canal (SC) Opening Radius[2]	SC Expansion at Posterior LC[28]	Strains
Central Lamina Cribrosa (LC)	Anterior Sclera (AS) Displacement	
Depth[3]	at 3.4 mm Ring[2]	<b>ONH Mechanical Properties</b>
Change in LC depth[3]	AS Displacement at 6.0 mm Ring[2]	LC modulus
Prelaminar Tissue (PLT) Thickness	AS Angle Change at 3.4 mm Ring[2]	Scleral Modulus
Change[2]	AS Angle Change at 6.0 mm Ring[2]	Scleral Structural
SC Expansion at Canal Opening[2]		Stiffness

or numerical modeling [1], [16]–[18]. Advances in optical coherence tomography (OCT) have enabled noninvasive *in vivo* measurement of deep structures of the ONH that were previously inaccessible (e.g., LC depth), as well as of some biomechanical effects of IOP (e.g., the changes in LC depth) [3], [19]. Nevertheless, it remains a challenge to measure *in vivo* most elements of LC biomechanics and mechanical properties.

We hypothesized that the complex intertwining of parameters and effects of IOP [1], [17], [18], [20] could be leveraged so that parameters measurable *in vivo* with an OCT could be used to predict the elusive but important ONH biomechanics and mechanical properties. Achieving this would greatly improve the ability to make patient-specific studies of the sensitivity to IOP and susceptibility to glaucoma. In this project we set out to test this hypothesis, and to determine the sensitivity of these predictions on the experimental measurements. Specifically, our objective was to construct statistical models using parameters that may be determined experimentally to predict ONH biomechanics and mechanical properties (Table I). There is no *a priori* reason to guarantee that the set of OCT-measurable parameters are sufficient to predict accurately all the outputs of interest. Hence, our first objective was to demonstrate that this is indeed the case. Our second objective was to carry out a parametric analysis and quantify the sensitivity of the predictions on the OCT-measurable measurements, and from this identify the experimental parameters that have the largest effects and are therefore central to understanding ONH biomechanics and tissue properties. Finally, a third objective was to integrate the statistical models into a software tool to allow quantitative estimates of our models quickly and easily.

Imaging of the posterior pole advances quickly and the set of parameters that are considered OCT-measurable increases often [2], [4], [22]–[27]. Thus, we considered two sets of parameters:

TABLE II

MODEL PARAMETERS AND THE RANGES OVER WHICH THEY WERE VARIED

Model Input	Minimum	Maximum
IOP	5.0 mmHg	15.0 mmHg
Eye Radius	9.6 mm	14.4 mm
Scleral Thickness	0.64 mm	0.96 mm
Anterior Lamina Cribrosa Radius	0.76 mm	1.14 mm
Neural Tissue Compressibility (Poisson's ratio)	0.4	0.49
Neural Tissue Modulus	0.01 MPa	0.09 MPa
Laminar Modulus	0.1 MPa	0.9 MPa
Scleral Modulus	1.0 MPa	9.0 MPa
Lamina Cribrosa Depth	0.0 mm	0.2 mm

TABLE III

DIRECT FE MODELING INPUTS AND OUTPUTS. DIRECT FE MODELING TAKES AS INPUTS GEOMETRY, MECHANICAL PROPERTIES, AND BOUNDARY CONDITIONS, AND PRODUCES AS OUTPUT THE LARGE AND SMALL SCALE DEFORMATIONS AND THE FORCES THROUGH THE TISSUES. COMPARING WITH TABLE I EXPOSES THAT NOT ALL INPUTS TO MODELING ARE MEASURABLE IN AN EXPERIMENT. COMPARING WITH TABLE I EXPOSES A FUNDAMENTAL CHALLENGE FOR UNDERSTANDING THE ONH *IN VIVO*: THE MISMATCH BETWEEN THE PARAMETERS MEASURABLE IN AN EXPERIMENT AND THOSE THAT DETERMINE ONH BIOMECHANICS (THE DIRECT FE MODEL INPUTS). TRADITIONALLY THIS HAS BEEN BRIDGED THROUGH INVERSE MODELING CASE-BY-CASE. HEREIN WE PROVIDE A GENERAL FRAMEWORK FOR DOING THIS IN THE ONH. AS: ANTERIOR SCLERA; SC: SCLERAL CANAL; LC: LAMINA CRIBROSA; PLT: PRELAMINAR TISSUE

Direct FE Model inputs	Direct FE Model outputs
IOP (both baseline and increase)	Stresses
Eye Radius	Strains
Anterior LC Radius	SC Expansion at Anterior LC
LC modulus	SC Expansion at Posterior LC
Scleral Modulus	AS Displacement at 3.4 mm Ring
Scleral Thickness	AS Displacement at 6.0 mm Ring
Neural Tissue Modulus	AS Angle Change at 3.4 mm Ring
SC Opening Radius	AS Angle Change at 6.0 mm Ring
Central LC Depth	Central LC Displacement
	PLT Thickness Change
	SC Expansion at Canal Opening

a *measurable* set of parameters that have consistently been reported in the peer-reviewed literature as measurable (Table I, leftmost column), and a *potentially measurable* set of parameters that have been proposed as measurable and in the next few years may be accepted as reliable by the community as technology and analysis progress (Table I, middle column).

## II. METHODS

Our general strategy was as follows: we built a set of 4646 finite element (FE) models representing a wide range of eye and ONH characteristics based on data from the literature or from our own measurements (Table II, sI) [13], [21], [29]. For each FE model we simulated the effects of an increase in IOP using direct FE modeling [21], [30], i.e., assuming tissue mechanical properties, anatomy and IOP (Direct FE model inputs in Table III), obtaining from the simulation measures of the effects of IOP (Direct FE model outputs in Table III). FE model inputs and outputs combined included all the outputs of interest, as well as the OCT-measurable parameters (both measurable and potentially measurable). We computed statistical models for each of the outputs of interest as a function of OCT-measurable

parameters. This step is equivalent to a regression of the predicted variable (an output of interest) as a function of multiple predictors (the measurable and potentially measurable parameters). Accurate fits thus demonstrating that the outputs of interest can be estimated from a given set of parameters. Once this had been achieved for all the outputs of interest we used the statistical models to evaluate the sensitivity of the predictions to variations in the measurable and potentially measurable parameters. Finally, the statistical models were integrated into a software platform for making quantitative predictions. The steps are described in detail below.

#### A. Model Construction and Simulation

The FE models were constructed and the effects of IOP simulated as described elsewhere (Fig. 1) [21]. Briefly, the models were simplified, generic and axisymmetric with a base model representing the ONH geometry at a low IOP of 5 mmHg. For this work we simulated a relatively modest IOP increase of 10 mmHg, which allowed modeling the tissues as linearly elastic, isotropic, and homogenous. Each tissue's behavior was governed by two parameters: a stiffness (Young's modulus) and a compressibility (Poisson's ratio). All tissues other than the pre-laminar neural tissue were modeled as incompressible. Note that, as before [31], [32], we use stiff to refer to tissues with a high Young's modulus, and compliant to refer to tissues with a low Young's modulus. Hence, in this paper stiffness is independent of geometry. We use structural stiffness as a parameter combining geometry and material properties, which has been found useful for the study of the scleral shell [33]. As elsewhere, we computed the scleral structural stiffness as the scleral modulus multiplied by scleral thickness [34], [35].

To parameterize the ONH anatomy and tissue properties we selected as model inputs nine characteristics previously identified as having the strongest influence on lamina stress, strain, and displacement (Table II) [17], [36], [37]. The set of cases was selected according to a response surface experimental design spreading parameter combinations throughout the space to balance uniform sampling density and ensure uniform quality of fit (minimizing the volume of the confidence ellipsoid for the coefficients), and a reasonable set size (Supplemental Fig. s2) [36]. This resulted in 4646 cases. The effects of an increase in IOP were simulated using commercial software as described elsewhere [21], [36] (Ansys 11; Ansys Inc., Canonsburg, PA, USA).

Twenty effects of IOP were measured for each model (Direct FE model outputs in Table III) [1]: The maximum tensile and compressive strains (the maximum and minimum principal strains, with compressive strains negative) [38], and the von Mises stress, which represents the forces acting through the tissue per unit area while discounting the effects of hydrostatic pressure [28], [30], [39]. To capture the variations of strains and stress over the tissues we computed the 50th and 95th percentiles. These represented the median and peak magnitudes, while reducing the influence of possible numerical artifacts [40] or effects of regions too small to have physiologic significance [38]. The stress and strain for the peripapillary sclera were calculated in a 5° region from the axis of symmetry to focus on the sclera immediately adjacent to the LC. Peak and median values

of two strains and a stress for each of the lamina cribrosa and sclera produced 12 responses for each model. We also computed the following geometrical measures (Fig. 1) [1].

- The anterior–posterior lamina cribrosa displacement, measured as the change in the anterior–posterior depth of the center point of the lamina cribrosa with respect to the anterior lamina insertion into the sclera [41].
- The prelaminar tissue thickness change, measured as the change in prelaminar tissue thickness at the center of the LC [13].
- The scleral canal expansion at the scleral canal opening, at the anterior lamina insertion, and at the posterior lamina insertion, measured as the changes in the scleral canal diameter at the three levels along the canal [14], [41].
- The anterior–posterior displacement of the peripapillary sclera at a distance 1.7 mm or 3.0 mm of the center of the scleral canal, measured as the anterior–posterior displacement of the anterior scleral surface at the specified distance.
- The angle change (rotation) of the peripapillary sclera at a distance 1.7 mm or 3.0 mm of the center of the scleral canal [2], [42], [43].

Measurements of displacement and angle change at 1.7 mm from the center of the canal were intended to capture peripapillary sclera bowing at a location comparable with the standard ring used for peripheral retinal nerve fiber layer thickness measurements [26]. Measurements at 3.0 mm from the center of the canal are expected to better represent a scleral response independent of the ONH.

#### B. Constructing the Statistical Models

This step is akin to a regression to determine the coefficients that optimize the closeness by which a function is “fit” to a set of points. When fitting data the functions to fit must be chosen carefully so as to have enough flexibility to capture the variations and complexity of the data, but not so much that it leads to “over-fit.” When over-fitting the predictions are highly accurate for the data used in fitting, but poor for other cases [44]. Optimal fits are done with the simplest possible function that closely approximates the data. Previously we had successfully fit ONH biomechanics data using third order polynomials [36]. In this work it was found that more flexible functions were needed (results not shown). For this we chose a method known as Multivariate Adaptive Regression Splines (MARS) [24], [27] (available in R v2.12.0) [45], [46]. MARS is an extension of linear regression that allows piecewise fits in multiple dimensions. In MARS over-fitting was prevented by penalizing the use of additional variables or terms, and evaluated as explained below. The models allowed up to third-order interactions. The nonlinear parameter relationships sometimes required transforming the parameters, for which we considered three transformations: logarithm base 10, square root, and square. These transformations belong to the Box-Cox family and are often used in design of experiments and response surface analysis studies to improve model fits and allow unbiased predictions in the presence of nonlinear relationships [47], [48]. Numerically this was a complication because the parameters sometimes take zero or negative values. For example, the LC displacement can be positive

(LC displacing posteriorly as IOP increases), negative (LC displacing anteriorly), or near zero. To deal with this for computing the logarithms and square roots we either took the negative of the parameter or added a constant (Supplementary Table s1). Two sets of prediction functions were computed: using only the measurable characteristics, and using both the measurable and potentially measurable characteristics. Using unpaired t-tests we evaluated if including the potentially measurable parameters significantly improved the fits.

To evaluate the quality of the fits, for accuracy and to avoid over-fitting, we computed generalized cross-validated  $R^2$ s calculated using ten-fold cross validation [44]. Briefly, this means that the fits were computed using a randomly selected subset of the data (in our case 90%), and the quality of the fit quantified by the residual obtained in predicting the rest of the data. For simplicity we refer to the cross-validated  $R^2$ s as  $R^2$ s. A prediction was considered satisfactory when the  $R^2$  was greater than 0.95. In addition to  $R^2$  we computed two other measures to describe the quality of the fits. First, 95E defined as the 95th percentile of the absolute value of the residual. 95E represents the width of a prediction made with 95% confidence in the units of the predicted parameter. Second, a ratio of the known ONH parameter range and the response spread (as defined in direct FE inputs) divided by 95E, rounded up. This ratio represents the number of classes that can be resolved, or bins in which the predictions can be classified. Typically as a fit improves  $R^2$  increases and 95E decreases, such that a perfect fit would have an  $R^2$  of 1.0, a 95E of 0.0, and we would be able to resolve an unlimited number of classes.

### C. Sensitivity Analysis

We used two methods to determine the output of interest sensitivities. For the first method we used the correlation matrix between parameters. The elements of this matrix represent a measure of the associations between variables over the whole parameter space, useful, as long as not interpreted as mechanistic. The correlation matrix was also used for dimensionality reduction (principal component analysis) on the output of interest to produce biplots. Biplots are a compact representation of the relationships between the parameters, simplifying visualization of the main parameter effects and the interactions between all parameters [1]. Readers unfamiliar with principal component analysis or biplots may want to consult the book by Everitt and Dunn [45]. Due to the multiple nonlinear parameter effects and the interactions between them, the response sensitivities and parameter influences varied substantially over the parameter space. To capture this complexity, in the second method, we used the statistical models to quantify the effects on the outputs of small changes ( $\pm 0.1\%$ ) in the measurable and potentially measurable parameters. By adding the effects over all the ONH models analyzed and normalizing by the total sensitivity of an output to all parameters we were able to obtain measures of overall parameter influences, as well as of the variability in these responses, in the same fashion as we did in a previous sensitivity studies [21], [31].

### D. Making Predictions Simple and Fast

We coded the statistical models into software following the general strategy described elsewhere [36].

TABLE IV

SUMMARY OF THE QUALITY OF FIT MEASURES FOR ALL THE OUTPUTS OF INTEREST. BETTER PREDICTIONS ARE REPRESENTED BY HIGHER  $R^2$ S AND SMALLER 95% CONFIDENCE WIDTHS (95E). RANGE/95E PROVIDES A SENSE OF THE SCALE OF THE ERROR (95E) RELATIVE TO THE OUTPUT RANGE. IT CAN BE INTERPRETED AS THE NUMBER OF "BINS" OR CLASSES INTO WHICH THE PREDICTIONS CAN BE RELIABLY SORTED, WITH MORE BINS INDICATING BETTER ABILITY TO DISCRIMINATE. FOR EXAMPLE, THE SMALLEST NUMBER OF BINS, TWO BINS FOR THE PREDICTIONS OF LC MODULUS USING ONLY MEASURABLE PARAMETERS (FIFTH ROW FROM THE TOP), INDICATES THAT USING ONLY MEASURABLE PARAMETERS IT IS ONLY POSSIBLE TO DISTINGUISH LCS INTO SOFT OR STIFF. ADDING THE POTENTIALLY MEASURABLE PARAMETERS IT IS POSSIBLE TO DISTINGUISH FOUR LC MODULUS GROUPS: SOFT, MEDIUM SOFT, MEDIUM STIFF, AND STIFF. MEASURABLE PARAMETERS WERE SUFFICIENT TO OBTAIN EXCELLENT PREDICTIONS OF THE SCLERAL MODULUS AND STRUCTURAL STIFFNESS, AS WELL AS FOR THE STRAINS. PREDICTIONS FOR THE LC MODULUS AND THE STRESSES BENEFITED MOST OF INCLUDING THE POTENTIALLY MEASURABLE PARAMETERS

		95% Confidence width (95E)			
		$R^2$	Range	Range/95E	
Scleral Structural Stiffness		0.990	1.16 MPa*mm	8.00 MPa*mm	7
		0.997	0.64 MPa*mm	8.00 MPa*mm	13
Scleral Modulus		0.961	2.60 MPa	8.00 MPa	4
		0.991	0.66 MPa	8.00 MPa	13
Lamina Modulus		0.844	0.56 MPa	0.80 MPa	2
		0.968	0.24 MPa	0.80 MPa	4
Peripapillary Sclera Tensile Strain	Median	0.989	0.11 %	1.33 %	12
	Peak	0.998	0.07 %	1.33 %	19
Lamina Cribrosa Tensile Strain	Median	0.987	0.26 %	2.89 %	12
	Peak	0.998	0.12 %	2.89 %	25
Lamina Cribrosa Compressive Strain	Median	0.994	0.26 %	3.88 %	16
	Peak	0.997	0.18 %	3.88 %	22
Peripapillary Sclera Compressive Strain	Median	0.988	0.48 %	4.97 %	11
	Peak	0.994	0.32 %	4.97 %	16
Peripapillary Sclera von Mises Stress	Median	0.993	0.46 %	7.09 %	16
	Peak	0.998	0.29 %	7.09 %	25
Lamina von Mises Stress	Median	0.991	0.62 %	8.26 %	14
	Peak	0.995	0.48 %	8.26 %	18
Lamina von Mises Stress	Median	0.986	0.22 %	1.67 %	8
	Peak	0.995	0.16 %	1.67 %	11
Lamina von Mises Stress	Median	0.988	0.31 %	2.51 %	8
	Peak	0.995	0.18 %	2.51 %	14
Lamina von Mises Stress	Median	0.831	2.1 kPa	12.6 kPa	6
	Peak	0.966	0.7 kPa	12.6 kPa	18
Lamina von Mises Stress	Median	0.842	4.6 kPa	30.1 kPa	7
	Peak	0.957	2.1 kPa	30.2 kPa	22
Lamina von Mises Stress	Median	0.888	3.6 kPa	28.0 kPa	8
	Peak	0.987	1.1 kPa	28.0 kPa	26
Lamina von Mises Stress	Median	0.831	4.9 Kpa	39.9 kPa	9
	Peak	0.966	1.3 kPa	39.9 kPa	31
		from Measurable parameters			
		from Measurable and Potentially Measurable parameters			

## III. RESULTS

Fits for all the outputs of interest were excellent, with  $R^2$ s between 0.957 and 0.998 (Table IV), demonstrating that it is possible to predict the outputs accurately using OCT-measurable and potentially measurable parameters. Fits improved significantly by including the potentially measurable parameters ( $P < 0.001$ , unpaired t-test). Fits for the stresses were the most complex, such that predictions in median peripapillary stress and peak LC stress, for example, utilized every measurable and potentially measurable parameter. Outputs could be classified in two bins or better using measurable parameters, and four bins or better when considering potentially measurable parameters. For brevity, details of the parameters used to obtain the optimal fits are provided in supplemental Fig. s3–s5.

The multiple measurable and potentially measurable parameters often represented similar aspects of the effects of IOP. This redundancy and the associations between parameters and ONH biomechanics and mechanical properties can be visualized using biplots with the experimental parameters plotted as covariates (Figs. 2 and 3). The first four principal components captured 96.3% of the variance combined (58.6, 22.4, 12.5, and

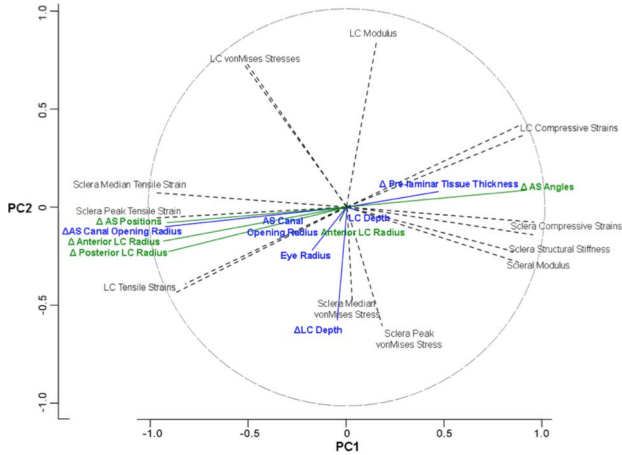


Fig. 2. Biplot of the two top principal components, PC1 and PC2. The plot shows a 2-D projection of the outputs of interest (dashed lines) and parameters (continuous lines, blue for measurable and green for potentially measurable parameters). The angle between lines represents the strength of the correlation between variables [1]. Strongly correlated variables are parallel ( $0^\circ$ ) or anti-parallel ( $180^\circ$ ), and independent variables are orthogonal ( $90^\circ$ ). All lines have a length of 1 in the multidimensional space of all PCs. Parameters are plotted as covariates and were not used to compute the PCs. PC1 was highly correlated with the sclera stiffness and strains. PC2 was highly correlated with LC stiffness and sclera stress. Notice the high correlation between various, measurable and potentially measurable, parameters of scleral deformation. The antiparallel relationship between laminar and sclera stresses suggests that “something must bear the loads.”

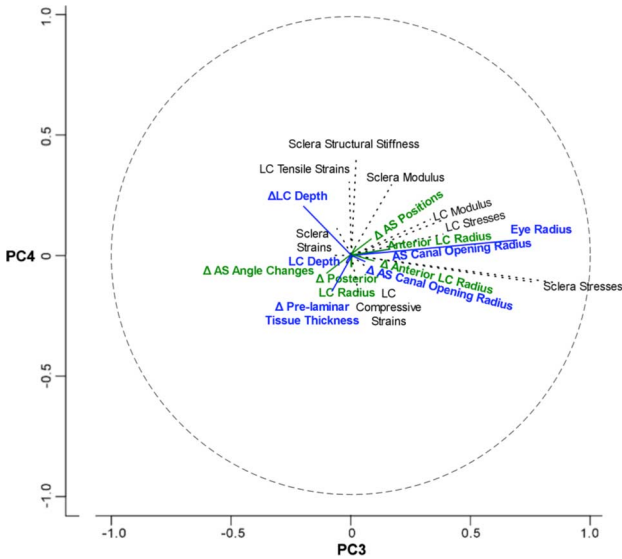


Fig. 3. Biplot of PC3 and PC4, with the same formatting as in Fig. 2. PC3 was highly correlated with globe size and sclera stresses, illustrating the high sensitivity of sclera stresses on the size of the eye. LC tensile strains were orthogonal to PC3 and increase with sclera stiffness (both modulus and structural).

2. 8%, respectively). The first two principal components were roughly aligned with the biomechanical properties of the sclera (PC1) and LC (PC2), whereas the third one was aligned with the size of the globe and the stresses within the sclera (PC3).

The sensitivities of predicted ONH biomechanics and properties to the measurable and potentially measurable parameters are summarized in Fig. 4. Forces through the LC and sclera were most sensitive to the sizes of the eye and canal (PCs 2 and 3 in Figs. 2 and 3). Tissue deformations (stretch and com-

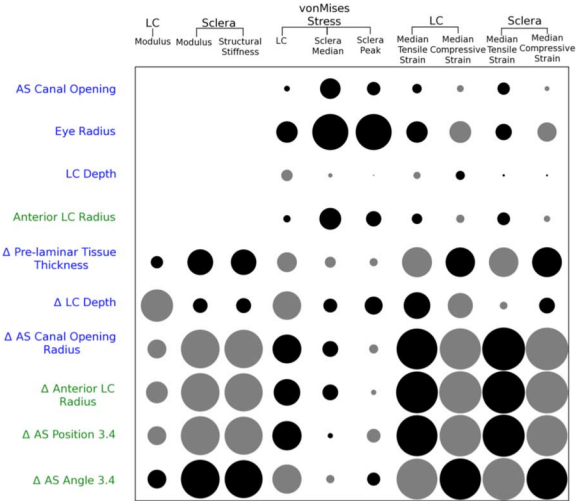


Fig. 4. Results from the sensitivity analysis. Relative sensitivity of estimated ONH mechanical properties and biomechanics (columns) on measurable (rows labeled in blue) and potentially measurable parameters (rows labeled in green). Disc areas are proportional to the percentage of an output variance due to each of the parameters, such that larger discs represent a stronger sensitivity of the response to the factor. Discs are black for positive covariations and gray for negative ones. The covariance and redundancy in parameters meant that sensitivity to one parameter implied some sensitivity to the covariates. Hence, multiple parameters shared influence patterns. Similarly, multiple outputs of interest had essentially the same parameter sensitivities. A representative set of outputs and parameters are shown, to avoid duplication and keep the plot clear. Note the strong sensitivities of estimated IOP-induced strains to parameters representing sclera deformations such as canal expansion.

pression) and biomechanical properties were highly sensitive to parameters representing effects of IOP on the sclera, including changes in canal radius at the opening or at the LC, as well as displacements and rotations away from the canal (PCs 1 and 2 in Fig. 2). Tissue mechanical properties were sensitive to dynamic effects of IOP: LC modulus was most sensitive to changes in LC depth, whereas sclera modulus and stiffness were most sensitive to deformations of the sclera. Note that, by design, gross tissue anatomy made no contribution to estimate the tissue mechanical properties as these were assumed independent in the initial parameterization. Predicted deformations and scleral properties were somewhat sensitive to changes in prelamellar tissue thickness.

The sensitivity analysis computed using small parameter variations produced similar results. Depending on whether the analysis included only measurable or potentially measurable the specific sensitivities varied slightly, but the overall patterns remained: ONH biomechanics were most sensitive to IOP-induced changes in canal width and anterior–posterior LC displacement. Because these results incorporate the nonlinear parameter interactions, the results are more comprehensive and complex, and therefore we present them as supplementary material (Figs. 6 and 7).

The statistical models were successfully implemented into an applet. With the applet it is quick and easy to obtain quantitative estimates of the outputs of interest (Fig. 5).

#### IV. DISCUSSION

We set out to test the hypothesis that parameters measurable *in vivo* using OCT can be used to estimate ONH biomechanics

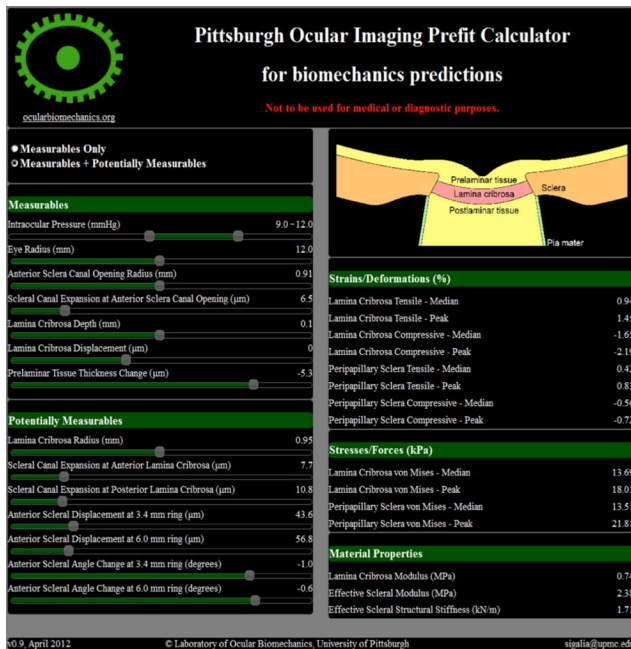


Fig. 5. Screenshot of the applet. On the left-hand side are the parameters, separated into measurable and potentially measurable. On the right-hand side the predicted ONH biomechanics and mechanical properties. A slider knob for each parameter allows setting the value (shown on the right hand side of the control). The applet allows selecting both baseline and increase in IOP, such that all predictions are increases relative to the baseline reference level. A warning is displayed if the parameters are selected outside the ranges used in our analysis, which would require an extrapolation, and is therefore highly unreliable.

and mechanical properties and, if so, to determine how these predictions are sensitive to the experimental measurements. Three main results arise from this work: 1) OCT-measurable parameters can be used to predict ONH biomechanics and mechanical properties; 2) predictions improve when also using potentially measurable parameters; and 3) predictions are highly sensitive to globe size and to IOP-induced changes in LC depth, scleral canal width, and prelaminar neural tissue thickness. Finally, we have introduced an applet, available online<sup>1</sup>, with which it is quick and easy to make predictions using the statistical models we have derived.

These results are important because ONH biomechanics and mechanical properties are potential biomarkers for sensitivity to IOP and susceptibility for development and progression of glaucoma [4], [5], [7], [8], [49]. The ability to estimate biomechanical effects of IOP and mechanical properties *in vivo* would greatly enhance the ability to test for the role of IOP on the development of glaucoma, as well as of the effects of the disease and in the evaluation of potential treatments [49]. The demonstration in this work using numerical models is a critical step. Previously we determined the sensitivity of ONH biomechanics to tissue anatomy and mechanical properties [21], [30], [32], [50], [51]. While insightful and meaningful from a fundamental perspective, those findings have been difficult to use in practice because most of the critical parameters remain unmeasurable *in vivo*. Here we present a method to predict the unmeasurable

parameters from the measurable ones, which should have a direct application in guiding and interpreting experiments. Estimates of IOP-induced stresses and strains will help evaluate the role of these insults on neural tissue degeneration in glaucoma, which has been the subject of substantial indirect analysis [4], [7], [18], [33], [36], [50], [52], [53]. Similarly, it would be useful in studies on the role of tissue mechanical properties on disease, which remains unclear, despite evidence that they are major determinants of the sensitivity to IOP [21], [30], [32], [50], [51] and change with disease [28], [33], [44], [54], [55] and aging [44], [53], [56], [57].

Others have used numerical modeling to estimate unmeasurable properties of ocular tissues based on measurable ones [18], [28], [33], [44], [53], [56]–[58]. The traditional approach has been to use a technique called inverse modeling. Our first objective can be rephrased as an inverse modeling problem, where we seek solutions for every case within a range of experimentally determined parameters. Instead of solving the inverse problem for each new case, we used a technique, pre-fitting. Pre-fitting is based on the concept of functional metamodeling that is well established within the larger field of optimization [59], but which is novel in ocular biomechanics. Differences between our technique and inverse modeling are summarized in Supplemental Fig. s8.

We would like to point out that our results are far from trivial, in that there was no *a priori* reason to guarantee that the parameters selected as measurable or potentially measurable would be sufficient to allow predicting accurately the outputs of interest. If, for example, we had only considered as measurable the changes in lamina cribrosa thickness, we would have been unable to obtain close predictions of sclera stiffness. Our process ensures that the predictions are consistent simultaneously with multiple experimentally-derived parameters and require that every parameter remains within the reasonable ranges we defined based on the literature. The predictions from our models should be considered as first-order estimates, useful for understanding gross characteristics of the ONH that cannot be measured in an experiment and an aid in interpreting the implications of variations in experiments. The estimates validity and accuracy are confined by the numerical models with which they were derived. We use the terms “prediction” and “estimate” to acknowledge the need for further experiments, which are in progress. In addition, we make our statistical models available as an easy to use applet to encourage evaluation of our predictions and comparison with experiments and with other models. We do not imply a temporal sense. Without comparison with measurements derived independently, our predictions or those obtained using inverse modeling [18], [28], [33], [44], [53], [56]–[58], should not be considered measurements. We recognize the potential risk that ease of use of the applet may lead some to dismiss the inherent assumptions and limitations. Users have used without trouble similar applet models published by our lab [36]. Experience with a previous applet [36] suggests that users recognize the challenges and appreciate the usefulness of the models without confusion. It should be noted that we are not proposing that simulations can be used to estimate ocular parameters without

<sup>1</sup>Available online: [ocularbiomechanics.org](http://ocularbiomechanics.org)

experimental measurements. The methodology we present is to use experimental data that is measurable or potentially measurable, to estimate data that remains unmeasurable. Use of the predictions from the methods we present should proceed carefully until they have been validated with independent experiments.

While each of our numerical models was relatively simple, our predictions incorporate the complex nonlinear multidimensional interplay between parameters [17], [36] and large-population effects [32], [37], [44], [60] that are often overlooked by other models of the ONH. Further, our models incorporate details of the peripapillary sclera, pre and postlaminal neural tissue, and pia mater typically missing in models focused on the complexity of the lamina or sclera. We present relatively gross parameters that we believe this type of model and analysis are appropriate to estimate.

The relationships determined in this work are not mechanistic, as they arise from regression and fitting. They should be seen as convenient numerical constructs that allow predicting unmeasurable outputs of interest from measurable parameters while simultaneously remaining consistent with multiple measurements. These considerations are not unlike the phenomenological constitutive models used to represent tissue mechanical properties [18], [28], [33], [44], [53], [56]–[58], which are useful even while not true to the anatomy and microstructure of the biological tissues. The consistency between parameters and predictions in our models ensured that the ranges of the predictions remained reasonable and in agreement with other modeling studies.

The most directly comparable experimental work is that on scleral stiffness of Girard and colleagues [34]. Varying the LC modulus from 0.1 to 1 MPa, they observed a maximum difference of 1 MPa on the predicted characteristics of the sclera, which was small compared with the range of sclera stiffnesses (Supplemental Fig. s1). The inaccuracy in our predictions of sclera properties was smaller than the imprecision in the inverse models of Girard *et al.*

For 95% of cases, we predicted the scleral modulus within 0.66 MPa, which is small enough to allow detection of the differences in scleral modulus observed due to aging. Girard *et al.* reported average moduli of 3.6, 6.5, and 8.8 MPa for the sclera of young, adult, and old monkeys, respectively (at 10 mmHg). The age-related changes (2.9 MPa and 2.3 MPa) are several times larger than the inaccuracy in our predictions. Predictions of tissue stiffness (Young's moduli) were accurate to 0.24 MPa for the LC. Predictions of ONH biomechanics were also highly accurate, with 95% confidence widths under 0.62% for strains and 4.9 kPa for the stresses. These widths were small enough to allow discerning predictions into multiple bins (2 to 31, depending on the predicted output).

Our results are evidence that current efforts to increase experimental capabilities are worthwhile, as all predictions improved significantly with the use of the potentially measurable parameters. Nevertheless, we found substantial redundancy within the measurable and potentially measurable parameters, which should be weighed when planning experiments to avoid wasted efforts [1].

Limitations of the modeling have been discussed [7], [21], [30], [36]. The models represented a generic simplified axisymmetric ONH without the complexities and details of specific ONHs [13], [15], [18], [20], [44], [51], [54], [61]–[63]. Sensitivity studies have shown that overall ONH biomechanics depend more strongly on the properties of the scleral shell than on the details of the anatomy and mechanical properties sclera [20], [21], [26], [33], [60]. These details, however, may be important in the local effects of IOP [64], [65]. The LC and sclera moduli we predict represent effective stiffnesses, in the same sense as done elsewhere, [18], [28], and should not be interpreted to represent the tissues away from the ONH, which varies in complex ways that our models did not consider [53], [66]. The tissues were modeled as linear, homogeneous, isotropic, and incompressible [21], [30]. Studies of ocular tissue properties have shown that the assumption of linearly elastic material properties is adequate at low levels of IOP (small deformations), but it becomes problematic for IOPs between 17 and 25 [53], [56], [67], [68]. Hence, our design using a relatively modest 10 mmHg increase in IOP with a maximum of 15 mmHg allowed us to use linear materials, for which models and analysis are much simpler. Estimates at higher IOPs would require models with nonlinear materials, which are the subject of substantial research efforts [18], [28], [33], [44], [53], [56]–[58]. A modest increase in IOP still within normal limits may be more easily achieved *in vivo* with low risk and without discomfort, and therefore may be more readily applicable in an experiment. We believe that studying normal IOP and small IOP elevations may be informative for understanding the pathogenesis of low-tension glaucoma. As we have demonstrated [1], [60] a solid understanding of ONH biomechanics at low pressures helps build an understanding at elevated IOPs. The models represent only an acute deformation of the tissues due to increases in IOP and do not account for long-term processes, such as remodeling [4], [5], [20]. Input factor ranges were based on the literature, including some data obtained from nonhuman samples, as well as a variety of methods of measurement (Supplemental Fig. s1).

In recent years evidence has been presented that the cerebrospinal fluid pressure within the subarachnoid space may also be a risk factor for glaucoma [69], [70]. Hence, an important improvement to this work could come from extending the models to include retrolaminar pressures.

The choice of outputs of interest and experimental parameters was based on our understanding of ONH biomechanics, of experiments on the posterior pole and on theories of glaucomatous optic neuropathy. For example, LC visibility in OCT remains highly variable despite advances such as enhanced depth imaging [71]–[73] and signal compensation algorithms [74]. We therefore chose to track gross lamina depth and displacement, as these may be more easily determined. The parameter ranges were defined to represent normal eyes, and the predictions obtained with them apply only to normal eyes.

## V. CONCLUSION

We have demonstrated that modeling techniques can be used to obtain from OCT images important biomechanical meaning that was previously not accessible *in vivo*. Estimates of ONH

biomechanics and mechanical properties have the potential to improve understanding of eye sensitivity to IOP and assessment of patient risk for development or progression of glaucomatous neuropathy.

## REFERENCES

- [1] D. C. Montgomery, *Design and Analysis of Experiments*. New York: Wiley, 2004.
- [2] Z. Nadler, B. Wang, G. Wollstein, D. Hammer, R. Ferguson, H. Ishikawa, R. Bilonick, J. Nevins, L. Kagemann, and J. Schuman, "Repeatability of three-dimensional (3D) microstructural parameters of the lamina cribrosa (LC) in adaptive optics spectral-domain optical coherence tomography (AO-SDOCT)," *Invest. Ophthalmol. Vis. Sci.*, vol. 54, 2013.
- [3] Y. Agoumi, G. P. Sharpe, D. M. Hutchison, M. T. Nicoleta, P. H. Artes, and B. C. Chauhan, "Laminar and prelaminar tissue displacement during intraocular pressure elevation in glaucoma patients and healthy controls," *Ophthalmology*, vol. 118, pp. 52–59, Jan. 2011.
- [4] C. F. Burgoyne, J. C. Downs, A. J. Bellezza, J. K. Suh, and R. T. Hart, "The optic nerve head as a biomechanical structure: A new paradigm for understanding the role of IOP-related stress and strain in the pathophysiology of glaucomatous optic nerve head damage," *Prog. Retin Eye Res.*, vol. 24, pp. 39–73, Jan. 2005.
- [5] H. A. Quigley, "Glaucoma: Macrocosm to microcosm the Friedenwald lecture," *Invest. Ophthalmol. Vis. Sci.*, vol. 46, pp. 2662–2670, Aug. 2005.
- [6] I. A. Sigal, "Interactions between geometry and mechanical properties on the optic nerve head," *Invest. Ophthalmol. Vis. Sci.*, vol. 50, pp. 2785–2795, Jun. 2009.
- [7] I. A. Sigal and C. R. Ethier, "Biomechanics of the optic nerve head," *Exp. Eye Res.*, vol. 88, pp. 799–807, Apr. 2009.
- [8] K. Takayama, M. Hangai, Y. Kimura, S. Morooka, M. Nukada, T. Akagi, H. O. Ikeda, A. Matsumoto, and N. Yoshimura, "Three-dimensional imaging of lamina cribrosa defects in glaucoma using swept-source optical coherence tomography," *Invest. Ophthalmol. Vis. Sci.*, vol. 54, pp. 4798–4807, Jul. 2013.
- [9] D. J. Brown, N. Morishige, A. Neekhra, D. S. Minckler, and J. V. Jester, "Application of second harmonic imaging microscopy to assess structural changes in optic nerve head structure ex vivo," *J. Biomed. Opt.*, vol. 12, p. 024029, Mar.–Apr. 2007.
- [10] I. A. Sigal and J. L. Grimm, "A few good responses: Which mechanical effects of IOP on the ONH to study?," *Invest. Ophthalmol. Vis. Sci.*, vol. 53, pp. 4270–4278, Jun. 2012.
- [11] D. B. Yan, F. M. Coloma, A. Methetairait, G. E. Trope, J. G. Heathcote, and C. R. Ethier, "Deformation of the lamina cribrosa by elevated intraocular pressure," *Br. J. Ophthalmol.*, vol. 78, pp. 643–648, Aug. 1994.
- [12] H. Yang, J. C. Downs, I. A. Sigal, M. D. Roberts, H. Thompson, and C. F. Burgoyne, "Deformation of the normal monkey optic nerve head connective tissue after acute IOP elevation within 3-D histomorphometric reconstructions," *Invest. Ophthalmol. Vis. Sci.*, vol. 50, pp. 5785–5799, Dec. 2009.
- [13] I. A. Sigal, J. G. Flanagan, I. Tertinegg, and C. R. Ethier, "3D morphometry of the human optic nerve head," *Exp. Eye Res.*, vol. 90, pp. 70–80, Jan. 2010.
- [14] M. D. Roberts, V. Grau, J. Grimm, J. Reynaud, A. J. Bellezza, C. F. Burgoyne, and J. C. Downs, "Remodeling of the connective tissue microarchitecture of the lamina cribrosa in early experimental glaucoma," *Invest. Ophthalmol. Vis. Sci.*, vol. 50, pp. 681–690, Feb. 2009.
- [15] J. Albon, W. S. Karwatowski, D. L. Easty, T. J. Sims, and V. C. Durance, "Age related changes in the non-collagenous components of the extracellular matrix of the human lamina cribrosa," *Br. J. Ophthalmol.*, vol. 84, pp. 311–317, Mar. 2000.
- [16] R. Grytz, I. A. Sigal, J. W. Ruberti, G. Meschke, and J. C. Downs, "Lamina cribrosa thickening in early glaucoma predicted by a microstructure motivated growth and remodeling approach," *Mech. Mater.*, vol. 44, pp. 99–109, Jan. 2012.
- [17] I. A. Sigal, "Interactions between geometry and mechanical properties on the optic nerve head," *Invest. Ophthalmol. Vis. Sci.*, vol. 50, pp. 2785–2795, Jun. 2009.
- [18] M. D. Roberts, Y. Liang, I. A. Sigal, J. Grimm, J. Reynaud, A. Bellezza, C. F. Burgoyne, and J. C. Downs, "Correlation between local stress and strain and lamina cribrosa connective tissue volume fraction in normal monkey eyes," *Invest. Ophthalmol. Vis. Sci.*, vol. 51, pp. 295–307, Jan. 2010.
- [19] Z. Nadler, B. Wang, G. Wollstein, J. E. Nevins, H. Ishikawa, L. Kagemann, I. A. Sigal, R. D. Ferguson, D. X. Hammer, I. Grulkowski, J. J. Liu, M. F. Kraus, C. D. Lu, J. Hornegger, J. G. Fujimoto, and J. S. Schuman, "Automated lamina cribrosa microstructural segmentation in optical coherence tomography scans of healthy and glaucomatous eyes," *Biomed. Opt. Exp.*, vol. 4, pp. 2596–2608, Nov. 2013.
- [20] T.-W. Kim, L. Kagemann, M. L. J. A. Girard, N. G. Strouthidis, K. R. Sung, C. K. Leung, J. S. Schuman, and G. Wollstein, "Imaging of the lamina cribrosa in Glaucoma: Perspectives of pathogenesis and clinical applications," *Current Eye Res.*, vol. 38, pp. 903–909, 2013.
- [21] I. A. Sigal, J. G. Flanagan, and C. R. Ethier, "Factors influencing optic nerve head biomechanics," *Invest. Ophthalmol. Vis. Sci.*, vol. 46, pp. 4189–4199, Nov. 2005.
- [22] H. Y. Park, S. H. Jeon, and C. K. Park, "Enhanced depth imaging detects lamina cribrosa thickness differences in normal tension glaucoma and primary open-angle Glaucoma," *Ophthalmology*, vol. 119, no. 1, pp. 10–20, Jan. 2012.
- [23] S. C. Park, C. G. De Moraes, C. C. Teng, C. Tello, J. M. Liebmann, and R. Ritch, "Enhanced depth imaging optical coherence tomography of deep optic nerve complex structures in Glaucoma," *Ophthalmology*, vol. 119, no. 1, pp. 3–9, Jan. 2012.
- [24] H. Y. Park and C. K. Park, "Diagnostic capability of lamina cribrosa thickness by enhanced depth imaging and factors affecting thickness in patients with glaucoma," *Ophthalmology*, vol. 120, pp. 745–752, Apr. 2013.
- [25] K. Takayama, M. Hangai, Y. Kimura, S. Morooka, M. Nukada, T. Akagi, H. O. Ikeda, A. Matsumoto, and N. Yoshimura, "Three-dimensional imaging of lamina cribrosa defects in glaucoma using swept-source optical coherence tomography," *Invest. Ophthalmol. Vis. Sci.*, vol. 54, pp. 4798–4807, Jul. 2013.
- [26] T. W. Kim, L. Kagemann, M. J. Girard, N. G. Strouthidis, K. R. Sung, C. K. Leung, J. S. Schuman, and G. Wollstein, "Imaging of the lamina cribrosa in glaucoma: Perspectives of pathogenesis and clinical applications," *Curr. Eye Res.*, vol. 38, pp. 903–909, Sep. 2013.
- [27] S. C. Park, S. Kiumehr, C. C. Teng, C. Tello, J. M. Liebmann, and R. Ritch, "Horizontal central ridge of the lamina cribrosa and regional differences in laminar insertion in healthy subjects," *Invest. Ophthalmol. Vis. Sci.*, vol. 53, pp. 1610–1616, Mar. 2012.
- [28] M. D. Roberts, I. A. Sigal, Y. Liang, C. F. Burgoyne, and J. C. Downs, "Changes in the biomechanical response of the optic nerve head in early experimental Glaucoma," *Invest. Ophthalmol. Vis. Sci.*, vol. 51, no. 11, pp. 5675–84, Nov. 2010.
- [29] M. J. A. Girard, J. C. Downs, M. Bottlang, C. F. Burgoyne, and J.-K. F. Suh, "Peripapillary and posterior scleral mechanics—Part II: Experimental and inverse finite element characterization," *J. Biomechan. Eng.*, vol. 131, p. 051012, 2009.
- [30] I. A. Sigal, J. G. Flanagan, I. Tertinegg, and C. R. Ethier, "Finite element modeling of optic nerve head biomechanics," *Invest. Ophthalmol. Vis. Sci.*, vol. 45, pp. 4378–4387, Dec. 2004.
- [31] I. A. Sigal, J. G. Flanagan, and C. R. Ethier, "Interactions between factors influencing optic nerve head biomechanics," presented at the Summer Bioeng. Conf., Keystone, CO, 2007.
- [32] B. Wang, Z. Nadler, J. Nevins, R. Bilonick, H. Ishikawa, L. Kagemann, I. Grulkowski, J. Liu, J. Fujimoto, and J. Schuman, "Automated segmentation of the in-vivo lamina cribrosa (LC) imaged using 3D optical coherence tomography (OCT)," *Invest. Ophthalmol. Vis. Sci.*, vol. 54, 2013.
- [33] M. J. Girard, J. K. Suh, M. Bottlang, C. F. Burgoyne, and J. C. Downs, "Biomechanical changes in the sclera of monkey eyes exposed to chronic IOP elevations," *Invest. Ophthalmol. Vis. Sci.*, vol. 52, no. 8, pp. 5656–69, Jul. 2011.
- [34] M. J. Girard, J. C. Downs, M. Bottlang, C. F. Burgoyne, and J. K. Suh, "Peripapillary and posterior scleral mechanics—Part II: Experimental and inverse finite element characterization," *J. Biomech. Eng.*, vol. 131, p. 051012, May 2009.
- [35] I. A. Sigal, M. D. Roberts, M. Girard, C. F. Burgoyne, and J. C. Downs, "Biomechanical changes of the optic disc," in *Ocular Disease: Mechanisms and Management*, L. A. Levin and D. M. Albert, Eds. New York: Elsevier, 2010.
- [36] I. A. Sigal, "An applet to estimate the IOP-induced stress and strain within the optic nerve head," *Invest. Ophthalmol. Vis. Sci.*, vol. 52, no. 8, pp. 5497–506, Jul. 2011.
- [37] I. A. Sigal, H. Yang, M. D. Roberts, C. F. Burgoyne, and J. C. Downs, "IOP-induced lamina cribrosa displacement and scleral canal expansion: An analysis of factor interactions using parameterized eye-specific models," *Invest. Ophthalmol. Vis. Sci.*, vol. 52, pp. 1896–1907, Mar. 2011.

- [38] I. A. Sigal, J. G. Flanagan, I. Tertinegg, and C. R. Ethier, "Predicted extension, compression and shearing of optic nerve head tissues," *Exp. Eye Res.*, vol. 85, pp. 312–322, 2007.
- [39] I. A. Sigal, J. G. Flanagan, I. Tertinegg, and C. R. Ethier, "Reconstruction of human optic nerve heads for finite element modeling," *Technol. Health Care*, vol. 13, pp. 313–329, 2005.
- [40] R. D. Cook, *Finite Element Modeling for Stress Analysis*. New York: Wiley, 1995.
- [41] I. A. Sigal, H. Yang, M. D. Roberts, and J. C. Downs, "Morphing methods to parameterize specimen-specific finite element model geometries," *J. Biomech.*, vol. 43, pp. 254–262, Jan. 19, 2010.
- [42] N. G. Strouthidis, B. Fortune, H. Yang, I. A. Sigal, and C. F. Burgoyne, "Longitudinal change detected by spectral domain optical coherence tomography in the optic nerve head and peripapillary retina in experimental glaucoma," *Invest. Ophthalmol. Vis. Sci.*, vol. 52, pp. 1206–1219, Mar. 2011.
- [43] B. Fortune, T. E. Choe, J. Reynaud, C. Hardin, G. A. Cull, C. F. Burgoyne, and L. Wang, "Deformation of the rodent optic nerve head and peripapillary structures during acute intraocular pressure elevation," *Invest. Ophthalmol. Vis. Sci.*, vol. 52, pp. 6651–6661, Aug. 2011.
- [44] I. A. Sigal, J. L. Grimm, N. J. Jan, K. Reid, D. S. Minckler, and D. J. Brown, "Eye-specific IOP-induced displacements and deformations of human lamina cribrosa," *Invest. Ophthalmol. Vis. Sci.*, vol. 55, pp. 1–15, Jan. 2014.
- [45] B. S. Everitt and G. Dunn, *Applied Multivariate Data Analysis*, 2nd ed. London, U.K.: Arnold, 2001.
- [46] I. Sigal, J. Grimm, N.-J. Jan, R. Bilonick, G. Wollstein, L. Kagemann, H. Ishikawa, J. Schuman, K. Davoli, and K. Lathrop, "IOP elevation reduces the waviness of the load bearing collagen fibers in the lamina cribrosa," *Invest. Ophthalmol. Vis. Sci.*, vol. 54, 2013.
- [47] D. C. Montgomery, *Design and Analysis of Experiments*. New York: Wiley, 2004.
- [48] M. J. Anderson and P. J. Whitcomb, *RSM Simplified: Optimizing Processes Using Response Surface Methods for Design of Experiments*. New York: Productivity Press, 2005.
- [49] N. G. Strouthidis and M. J. Girard, "Altering the way the optic nerve head responds to intraocular pressure—A potential approach to glaucoma therapy," *Curr. Opin. Pharmacol.*, vol. 13, pp. 83–89, Feb. 2013.
- [50] I. A. Sigal, J. G. Flanagan, I. Tertinegg, and C. R. Ethier, "Modeling individual-specific human optic nerve head biomechanics. Part I: IOP-induced deformations and influence of geometry," *Biomech. Model Mechanobiol.*, vol. 8, pp. 85–98, Apr. 2009.
- [51] I. A. Sigal, J. G. Flanagan, I. Tertinegg, and C. R. Ethier, "Modeling individual-specific human optic nerve head biomechanics. Part II: Influence of material properties," *Biomech. Model Mechanobiol.*, vol. 8, pp. 99–109, Apr. 2009.
- [52] J. C. Downs, M. D. Roberts, and I. A. Sigal, "Glaucomatous cupping of the lamina cribrosa: A review of the evidence for active progressive remodeling as a mechanism," *Exp. Eye Res.*, Aug. 2010.
- [53] M. J. Girard, J. K. Suh, M. Bottlang, C. F. Burgoyne, and J. C. Downs, "Scleral biomechanics in the aging monkey eye," *Invest. Ophthalmol. Vis. Sci.*, Jun. 2009.
- [54] R. Grytz, M. A. Fazio, M. J. Girard, V. Libertiaux, L. Bruno, S. Gardiner, C. A. Girkin, and J. C. Downs, "Material properties of the posterior human sclera," *J. Mech. Behav. Biomed. Mater.*, Apr. 2013.
- [55] I. A. Sigal and C. R. Ethier, "Biomechanics of the optic nerve head," *Exp. Eye Res.*, vol. 88, pp. 799–807, 2009.
- [56] M. A. Fazio, R. Grytz, J. S. Morris, L. Bruno, S. K. Gardiner, C. A. Girkin, and J. C. Downs, "Age-related changes in human peripapillary scleral strain," *Biomech. Model Mechanobiol.*, Jul. 30, 2013.
- [57] B. Geraghty, S. W. Jones, P. Rama, R. Akhtar, and A. Elsheikh, "Age-related variations in the biomechanical properties of human sclera," *J. Mech. Behav. Biomed. Mater.*, vol. 16, pp. 181–191, Dec. 2012.
- [58] S. L. Woo, A. S. Kobayashi, W. A. Schlegel, and C. Lawrence, "Non-linear material properties of intact cornea and sclera," *Exp. Eye Res.*, vol. 14, pp. 29–39, Aug. 1972.
- [59] J. P. C. Kleijnen, *Design and Analysis of Simulation Experiments*. New York: Springer, 2007.
- [60] I. A. Sigal, J. G. Flanagan, I. Tertinegg, and C. R. Ethier, "Modeling individual-specific human optic nerve head biomechanics. Part I: IOP-induced deformations and influence of geometry," *Biomech. Model Mechanobiol.*, vol. 8, pp. 85–98, 2009.
- [61] B. Coudrillier, C. Boote, H. A. Quigley, and T. D. Nguyen, "Scleral anisotropy and its effects on the mechanical response of the optic nerve head," *Biomech. Model Mechanobiol.*, vol. 12, no. 5, pp. 941–63, Oct. 2013.
- [62] M. D. Roberts, R. T. Hart, Y. Liang, A. Bellezza, C. F. Burgoyne, and J. C. Downs, "Continuum-level finite element modeling of the optic nerve head using a fabric tensor based description of the lamina cribrosa," presented at the ASME Summer Bioeng. Conf., Keystone, CO, 2007.
- [63] J. Albon, P. P. Purslow, W. S. Karwatowski, and D. L. Easty, "Age related compliance of the lamina cribrosa in human eyes," *Br. J. Ophthalmol.*, vol. 84, pp. 318–323, Mar. 2000.
- [64] R. Grytz, I. A. Sigal, J. W. Ruberti, G. N. Meschke, and J. C. Downs, "Lamina cribrosa thickening in early glaucoma predicted by a microstructure motivated growth and remodeling approach," *Mechan. Mater.*, vol. 44, pp. 99–109, 2012.
- [65] M. D. Roberts, Y. Liang, I. A. Sigal, J. Grimm, J. Reynaud, A. Bellezza, C. F. Burgoyne, and J. C. Downs, "Correlation between local stress and strain and lamina cribrosa connective tissue volume fraction in normal monkey eyes," *Invest. Ophthalmol. Vis. Sci.*, vol. 51, pp. 295–307, Jan. 2010.
- [66] R. E. Norman, J. G. Flanagan, S. M. Rausch, I. A. Sigal, I. Tertinegg, A. Eilaghi, S. Portnoy, J. G. Sled, and C. R. Ethier, "Dimensions of the human sclera: Thickness measurement and regional changes with axial length," *Exp. Eye Res.*, vol. 90, pp. 277–284, Feb. 2010.
- [67] E. Spoerl, A. G. Boehm, and L. E. Pillunat, "The influence of various substances on the biomechanical behavior of lamina cribrosa and peripapillary sclera," *Invest. Ophthalmol. Vis. Sci.*, vol. 46, pp. 1286–1290, Apr. 2005.
- [68] A. Elsheikh, B. Geraghty, D. Alhasso, J. Knappett, M. Campanelli, and P. Rama, "Regional variation in the biomechanical properties of the human sclera," *Exp. Eye Res.*, vol. 90, pp. 624–633, May 2010.
- [69] J. P. Berdahl and R. R. Allingham, "Cerebrospinal fluid pressure may play a role in reversal of cupping after glaucoma surgery," *Am. J. Ophthalmol.*, vol. 148, pp. 623–624, Oct. 2009, author reply 624-5.
- [70] J. P. Berdahl, R. R. Allingham, and D. H. Johnson, "Cerebrospinal fluid pressure is decreased in primary open-angle glaucoma," *Ophthalmology*, vol. 115, pp. 763–768, May 2008.
- [71] I. C. Campbell, B. Coudrillier, and C. R. Ethier, "Biomechanics of the posterior eye: A critical role in health and disease," *J. Biomech. Eng.*, Dec. 1, 2013.
- [72] Y. Agoumi, G. P. Sharpe, D. M. Hutchison, M. T. Nicoleta, P. H. Artes, and B. C. Chauhan, "Laminar and prelaminar tissue displacement during intraocular pressure elevation in glaucoma patients and healthy controls," *Ophthalmology*, vol. 118, pp. 52–59, 2011.
- [73] C. F. Burgoyne, J. C. Downs, A. J. Bellezza, J.-K. F. Suh, and R. T. Hart, "The optic nerve head as a biomechanical structure: A new paradigm for understanding the role of IOP-related stress and strain in the pathophysiology of glaucomatous optic nerve head damage," *Progr. Retinal Eye Res.*, vol. 24, pp. 39–73, 2005.
- [74] M. J. Girard, N. G. Strouthidis, C. R. Ethier, and J. M. Mari, "Shadow removal and contrast enhancement in optical coherence tomography images of the human optic nerve head," *Invest. Ophthalmol. Vis. Sci.*, vol. 52, no. 10, pp. 7738–48, Sep. 2011.